PHYSICAL REVIEW A **92**, 033852 (2015)

Measurement of a subpicosecond coherence time in a quasi-steady-state XUV laser

Andréa Le Marec,* Limin Meng,† and Annie Klisnick
CNRS, Université Paris-Sud, ISMO UMR 8214, F-Orsay, France

Michaela Kozlova and Jaroslav Nejdl
IoP ASCR, ELI Beamlines Project, CZ-Prague, Czech Republic
and IPP ASCR, CZ-Prague, Czech Republic

Fabien Tissandier
ENSTA ParisTech, CNRS, Ecole Polytechnique, LOA UMR 7639, F-Palaiseau, France

Olivier Guilbaud
CNRS, Université Paris-Sud, LPGP UMR 8214, F-Orsay, France

Annette Calisti
Aix Marseille Université, CNRS, PIIM UMR 7345, F-Marseille, France
(Received 8 July 2015; published 28 September 2015)

We have carried out a detailed characterization of the temporal coherence and spectral bandwidth of the Ne-like Zn XUV laser, collisionally pumped in the quasi-steady-state (QSS) regime and operated at saturation. The measured coherence time $\tau_c = 680 \pm 70$ fs is significantly shorter than previously observed with other types of collisional XUV lasers, using the same measurement technique. Additional measurements performed below saturation were used to investigate gain narrowing of the spectral width of the lasing line. Our experimental data are well reproduced by calculations performed with a one-dimensional radiative transfer numerical code, taking the measured gain as an input. We show that our results are consistent with spectral measurements of QSS XUV lasers reported by different authors in the 1990s, although they were based on slightly different pumping conditions and measurement techniques.

DOI: 10.1103/PhysRevA.92.033852 PACS number(s): 42.55.Vc

I. INTRODUCTION

The last 10–15 years have seen the emergence of bright coherent sources in the extreme ultraviolet (XUV) range based on free-electron lasers (FEL) [1,2], high-order harmonic generation (HHG) [3], and plasma-based XUV lasers [4]. XUV FELs have achieved extremely high focused intensities with which new regimes of interaction with matter are now explored [5,6]. HHG sources can deliver ultrashort attosecond pulses, allowing one to investigate the electron dynamics of fundamental processes in atoms, molecules or surfaces [7–9]. Plasma-based XUV lasers, generated by collisional excitation pumping in plasmas produced from high power lasers or fast electrical discharges, have slightly different but complementary characteristics. They have been used for a broad range of applications including dense plasma diagnostics [10–12], nanopatterning [13], or photoionization of molecular clusters [14]. Depending on the technique used to generate the plasma amplifier, the output energy varies from $\sim 1 \mu$J to several mJ with pulse durations ranging from ~ 1 ps to ~ 1 ns. Recent advances in the development of these sources include operation at an increased repetition rate of 100 Hz [15], tailoring of the driving laser pulse to improve the pumping efficiency [16,17], or saturated operation below 10 nm with a compact laboratory-scale laser driver [18]. Another major step forward has been achieved with the demonstration and subsequent development of injection-seeded XUV lasers. In the seeded mode, a femtosecond HH pulse, resonant with the XUV laser line, is injected at one end of the pumped plasma, which acts as an amplifier. The properties of the output amplified beam are dramatically improved over the unseeded, amplification of the spontaneous emission (ASE) mode, with a significantly reduced divergence, improved wavefront and spatial coherence, and a defined linear polarization [19,20]. Seeding was also considered and recently demonstrated for free-electron lasers to overcome the significant shot-to-shot variation of the temporal shape of the pulse induced by the so-called SASE operation mode [2,21].

Following the first demonstration with weak amplification in 1995 [22], strong amplification of an HHG seed pulse has been achieved in two types of collisionally pumped XUV plasma amplifiers: optical-field ionized plasmas from gaseous targets [23] and transient pumping plasmas from solid targets [24,25]. In both cases the duration of the amplified seed pulse, which was directly measured [26] or indirectly estimated [27], was of ~ 1 to few picoseconds, significantly longer than the initial HH pulse (~ 30 fs). This temporal broadening is the result of the strong spectral narrowing experienced by the broadband HH pulse as it enters the plasma and is then amplified within the narrow gain bandwidth associated with the XUV laser line [28]. Enlarging the spectral bandwidth of XUV laser amplifiers is thus a requirement in order to preserve the femtosecond time scale of the amplified pulse. The spectral bandwidth

*andrea.le-marec@u-psud.fr
†Present address: Institute of Fluid Physics, China Academy of Engineering Physics, Mianyang, China.

mismatch between seed and amplifier was also shown from numerical simulations to control the onset of a dynamical regime of amplification [29], leading to Rabi oscillations with period of a few tens of femtoseconds and subsequent modulations in the amplified XUV pulse temporal and spectral profiles. It is thus important to have a detailed knowledge of the spectral properties of the different types of XUV lasers, which have been or could be considered for seeding. Using a wavefront-division interferometer specifically designed for that purpose [30], temporal coherence and corresponding spectral linewidth of three types of collisional XUV lasers have been characterized at different laboratories over the last few years: OFI-pumped Ni-like Kr ($\lambda = 32.8$ nm) [27], transient Ni-like Mo ($\lambda = 18.9$ nm) [31], and capillary-discharge Ne-like Ar ($\lambda = 46.9$ nm) [32]. The measured frequency linewidths $\Delta\nu$ (FWHM) range from 7.5×10^{10} Hz for the OFI Kr pumped laser, to 2.3×10^{11} Hz for the capillary-discharge Ar laser. The associated Fourier-transform limit durations (i.e., the ultimate minimum duration achievable) corresponding to these values are of ~5 ps and ~2 ps, respectively, and they are consistent with the measured durations of seeded XUV lasers mentioned above.

As discussed in [33], a promising way to enlarge the spectral bandwidth of the plasma amplifier would be to increase the electron density in the amplifier, inducing a proportional increase of the contribution of collisional broadening to the overall line profile. Such an increase of the electron density was successfully achieved for the OFI-pumped Kr laser using a preformed plasma waveguide [34]. For transient pumping XUV lasers, a frequency-doubled driving laser could be used to induce the required heating at a higher electron density, as suggested in [26]. Finally, collisional XUV lasers pumped in the quasi-steady-state (QSS) regime, such as the Ne-like zinc laser discussed in this paper, were also considered in numerical simulations as a promising way to achieve a very high peak power of multitens of GW, using a chirped picosecond HH pulse to extract the ~mJ energy stored in those systems [35]. Since QSS pumped XUV lasers are generated from a relatively long ~500-ps driving pulse incident at normal incidence on the target, they operate at both higher electron density and higher ionic temperature compared to the other types of collisional XUV lasers. As a result, the contributions of both collisional and Doppler broadenings to the overall linewidth are expected to be larger. With the motivation to provide experimental benchmarking to numerical simulations, we have carried out an experiment aimed at characterizing the spectral bandwidth of the QSS Ne-like Zn emitting at 21.2 nm, which is generated at the Prague Asterix Laser System (PALS) facility in Prague, Czech Republic [36]. We performed a preliminary experiment in 2012 [37], that indicated that the spectral bandwidth $\Delta\nu$ was actually larger than that of the other types of XUV lasers. However, due to some experimental difficulties, which will be explained below, the experimental arrangement was subsequently improved, and a new measurement campaign was carried out. The obtained results, described in this paper, not only provide a refined and more reliable measurement, but are further supported by the observation of gain narrowing of the XUV laser linewidth below and at saturation, and by a comparison to the predictions of numerical simulations.

In Sec. II, we briefly recall the main features of the QSS-pumped Ne-like Zn laser generated at PALS. We then describe the wavefront interferometer and the method that was used to measure the temporal coherence of this laser, from which its spectral linewidth was inferred. In Sec. III, we present the results of the measurement performed on the double-pass operated, fully saturated, zinc laser. The measured coherence time is found to be shorter by factors ranging from 2.6 to 8 than those previously measured, with the same instrument, with other types of collisional XUV lasers. The inferred spectral width is consistent with earlier measurements performed independently in other laboratories for QSS-pumped XUV lasers emitted at slightly different wavelengths. In Sec. IV, we present additional measurements performed in the single-pass configuration, where the zinc laser operates in the small-signal gain regime, below saturation. The experimental data are well reproduced by the predictions of numerical simulations based on a frequency-dependent, one-dimensional radiative transfer model. We show that a femtosecond broadband HH pulse injected in the Ne-like Zn amplifier would retain a pulse duration significantly below 1 ps (namely ~500 fs).

II. EXPERIMENTAL SETUP AND METHOD

The QSS Ne-like zinc laser characterized in this work emits at $\lambda = 21.22$ nm (transition $(2p^5_{1/2}3p_{1/2})_{J=0} \rightarrow (2p^5_{1/2}3s_{1/2})_{J=1}$). The conditions of generation and the main characteristics of this source are described in detail in [36]. The amplifier plasma is generated by irradiating a 3-cm-long zinc slab target with the PALS iodine laser at fundamental wavelength (1.315 μm) in a pump sequence composed of an ~2J–300-ps prepulse followed after 10 ± 0.5 ns by a ~600 J–350-ps main pulse. A population inversion is achieved in the spatial region slightly below the plasma critical density ($N_c = 6.5 \times 10^{20}\text{cm}^{-3}$) and temporally close to the peak of the main pulse, when the plasma temperature is maximum. The plasma conditions in the gain zone are not known precisely, but estimated as $N_e \sim$ 2–5 $\times 10^{20}\text{cm}^{-3}$; $\text{kT}_\text{e} =$ 200–300 eV; $\text{kT}_\text{i} =$ 150–200 eV from numerical simulations [38]. Due to the relatively long-lasting (~100 ps) and low gain (few cm^{-1}) typically obtained in this QSS pumping regime, saturation is achieved using a half-cavity allowing a double pass in the amplifier [36]. The half-cavity consisted of a Mo:Si flat multilayer mirror with 30% reflectivity around 21 nm placed at a distance of ~7 mm from the target. The zinc laser can also be operated in single pass by shifting the half-cavity mirror out of the XUV laser beam path. Figure 1 shows the experimental setup with the different diagnostics implemented along the XUV laser beamline. The spectral width of the zinc laser line was inferred from the temporal coherence of the XUV laser pulse, measured through a first-order autocorrelation of the XUV laser field. We used a dedicated wavefront-division interferometer with variable path difference, designed and fabricated at Institut d'Optique, Orsay, France, a decade ago. This interferometer is based on a pair of highly polished, flat roof-shaped mirrors arranged in a Fresnel-like geometry [39]. The mirrors are slightly tilted towards each other (tilt angle $\theta \sim$ 1–2 mrad) along their common edge. After reflection under a grazing angle of $\alpha = 6^\text{o}$ the XUV laser beam is thus divided into two half-beams that partially overlap. Interference

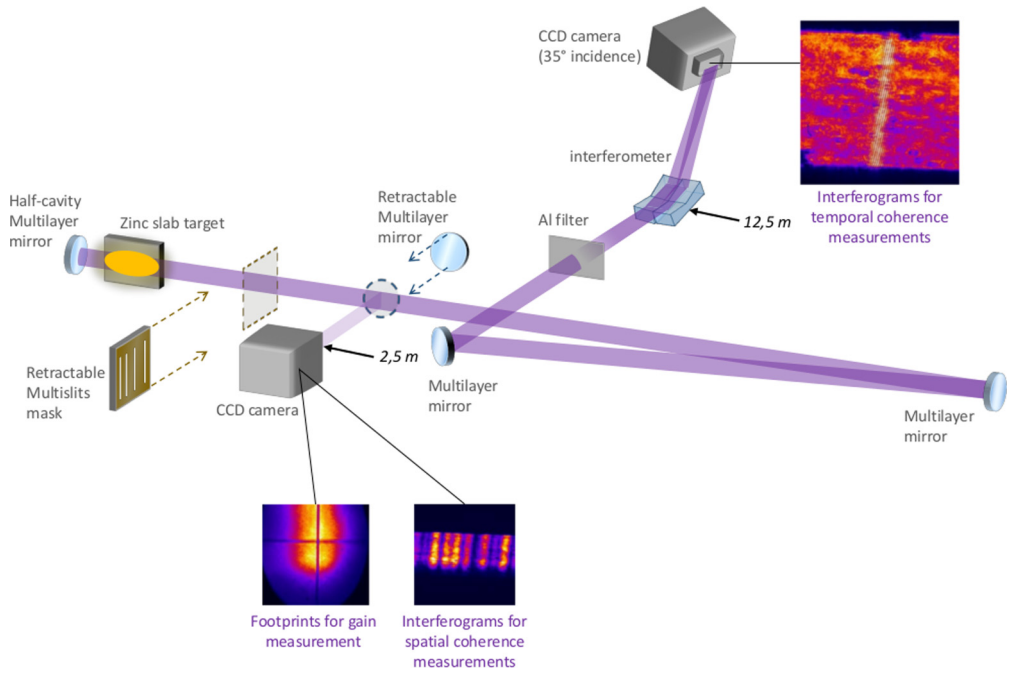

FIG. 1. (Color online) Experimental setup showing the path of the double-pass zinc XUV laser beam to the wavefront-division interferometer. A distance of 12.5 m from the source was required to optimize the maximum fringe visibility. The beam path was folded with two flat Mo:Si multilayer mirrors used at near-normal and 45° incidence, respectively. A footprint monitor and a spatial coherence diagnostic could be inserted in the beam path for additional beam characterization.

fringes are formed in the overlapping region and detected on a back-illuminated XUV CCD. In order to increase the apparent fringe spacing to ∼5 pixels/fringe, the camera is tilted to be hit at an incidence angle $\beta = 35^{\circ}$. The fringe spacing is given by $i = \lambda/\varepsilon \times (D + d)/(D \sin(\beta))$, where $D = 1200$ cm (respectively, $d = 750$ cm) is the distance from the roof-shaped mirrors to the XUV laser output plane (respectively, to the detector) and ε is the angle between the interfering beams: $\varepsilon = 4\alpha\theta \approx 0.54$ mrad in the present case. One of the roof-shaped mirrors is mobile and can be accurately translated in the vertical direction z to induce a controlled longitudinal path difference $\Delta\ell$, or delay τ, between the interfering half-beams, given by $\Delta\ell = c\tau = 2\Delta z \sin(2\alpha)$, where Δz is the mirror displacement. The use of roof-shaped mirrors with two reflections in each interferometer arm, instead of simple flat mirrors, ensures that the transverse distance between the overlapping points in each half-beam remain unchanged when varying the path difference. Hence, the variation of fringe visibility induced by the delay between the interfering beams is solely due to the finite temporal coherence of the XUV pulse, at a fixed degree of spatial coherence. A similar method involving wavefront division and temporal delay with slightly different design geometries was used at the FLASH free-electron laser facility to characterize the temporal coherence of the XUV pulse at several wavelengths [40,41]. Compared to these systems, the main originality of our instrument lies in a single-piece interfering element, contained in a compact vacuum chamber, hence allowing a relatively easy implementation in different laboratories. The degree of spatial coherence of the XUV laser beam at the position of the interferometer controls the maximum fringe visibility at zero path difference. This reference position of the interferometer was accurately determined (within a few fs accuracy) prior to the experimental campaign. In the ASE mode, the degree of spatial coherence of XUV lasers is limited, leading to maximum visibilities smaller than 100%. The spatial coherence length increases with the distance from the source, hence allowing one to a certain extent to adapt the distance with the desired maximum visibility. In the first experimental campaign performed at PALS the interferometer was implemented at distances of 5–7 m from the source, based on an earlier estimation of the spatial coherence length. However, the maximum visibility did not exceed 30% which severely limited the quality of the measurements [37]. During the second experiment, the distance was increased to 12.5 m, through folding the XUV laser beam path with two Mo:Si multilayer mirrors, as shown in Fig. 1. With such a large distance, the maximum visibility could be increased to ∼50–60%, as will be shown in the next section. Moreover, a multislit array with different separations could be inserted in the beam path to record a single-shot diffraction pattern on an XUV CCD camera at 2.5 m from the source [42]. This diagnostic was used to verify that the degree of spatial coherence did not vary significantly from one shot to the other, since this is a strong requirement in our measurement based on a multishot delay scan.

The image in the upper right part of Fig. 1 shows the fringe pattern from a typical single-shot interferogram recorded with the tilted CCD camera. The transverse size of the overlapping zone is $\Delta X = \varepsilon d \approx 400$ μm (≈700 μm in the CCD detector plane), which is approximately 1/150 of the transverse beam size at the detection plane, owing to the beam divergence of ∼5 mrad in the horizontal direction. Each interferogram obtained at a given delay τ between the interfering beam is then numerically processed, by applying a fast Fourier

transform (FFT) of the signal in a small sliding window over the region containing the interference fringes, after background subtraction. This yields a two-dimensional map of the fringe visibility $V(x,y,\tau)$, where in each window the visibility is calculated from $V = 2.S_1/S_0$ where S_1 the first-order peak (corresponding to the fringe modulation) and S_0 is the zero-order peak of the FFT signal in the spatial frequency domain. For a quasimonochromatic radiation the visibility of the interference fringes is related to the modulus of the complex degree of coherence $|\gamma_{12}(\tau)|$ through $V(\tau) = 2\sqrt{I_1 I_2}/I_1 + I_2|\gamma_{12}(\tau)|$. The ratio preceding $|\gamma_{12}(\tau)|$ introduces a correction by a factor <1 when the intensities I_1, I_2 of the interfering beams are unbalanced. Since the XUV laser beam is not spatially uniform, but exhibits structures on a spatial scale smaller than the overlapping zone, the visibility map is not uniform either, but displays variations of typically $\pm 10\%$. We assume that within the small overlapping region sampled by the interferometer the degree of spatial coherence of the beam is constant, so that the variations of fringe visibility are only caused by randomly distributed beam nonuniformities. Since the visibility is maximum when $I_1 = I_2$ we identify the maximum value of the measured visibility over the fringe zone to the modulus of the degree of coherence for the given delay τ. We further check in the visibility map and in the corresponding histogram that this value is not an "accident," i.e., that it occurs in a significant number of pixels.

The measurement of the coherence time τ_c of the zinc XUV laser pulse was performed by acquiring a series of single-shot interferograms for several temporal delays between -300 fs and $+1$ ps and by plotting the measured visibilities $V(\tau)$. We use the definition of the coherence time τ_c as the temporal delay between the interfering beams at which the fringe visibility $V(\tau)$ is reduced by a factor $1/e$ of its maximum value $V(0)$. It should be noted that within the small spectral bandwidth ($\Delta\lambda \approx 3$ nm) defined by the Mo:Si multilayer mirrors and the aluminum filter used, the incoherent, long-lasting thermal emission from the plasma adds an unknown contribution to the interference signal that cannot be subtracted. However, it can be easily shown that, if this incoherent emission is uniform over the fringe zone, it reduces the fringe visibility by a constant factor, which does not depend on the temporal delay τ. Thus, the contribution of incoherent thermal plasma emission may partly explain why the fringe visibility did not exceed $\sim 60\%$, even at 12.5 m from the source. However, this contribution does not affect our measurement of the coherence time.

The spectral width of the zinc XUV laser line is then inferred by first fitting the experimental data V(τ) with an appropriate analytical function (Gaussian in the present case). Following the Wiener-Khintchin theorem, the spectral power density and the complex degree of coherence are the Fourier transform pairs. As a result, the frequency linewidth $\Delta\nu$ [full width at half maximum (FWHM)] is related to the coherence time τ_c defined above by $\Delta\nu = 2\sqrt{\ln 2}/\pi\tau_c = 0.53/\tau_c$ for a Gaussian visibility curve (and corresponding Gaussian spectral profile).

III. LINEWIDTH OF THE DOUBLE-PASS SATURATED LASER

A first series of measurements was carried out with the zinc laser operated in double pass. In this case, as will be shown below, the amplification reaches saturation. Figure 2 summarizes the values of visibility measured from each single-shot interferogram for increasing values of the temporal delay. In spite of the limited number of shots in a series, the data can be well fitted with a Gaussian function, which is shown by the dotted line in Fig. 2. As already mentioned in the previous section, the maximum visibility at zero temporal delay is relatively low, slightly larger than 50%.

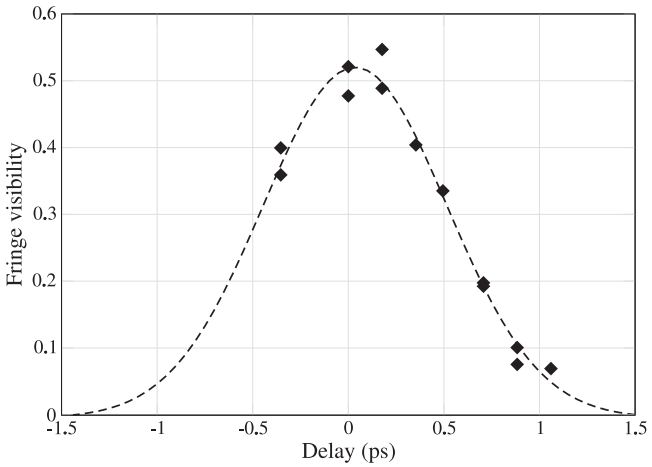

FIG. 2. Measured fringe visibility as a function of the temporal delay for the double-pass, 3-cm plasma length configuration. Each data point (solid diamonds) was measured in a single-shot interferogram.

The coherence time, defined as the temporal delay at which the visibility drops by $1/e$, is measured as $\tau_c = 680 \pm 70$ fs. Such a value is consistent with one of the measurements performed during the first experimental campaign at PALS ($\tau_c \sim 0.7$ ps [37]). This confirms that the coherence time of the saturated QSS zinc laser is significantly shorter that those previously measured for other types of collisional XUV lasers using the same instrument. They ranged from 1.8 ps for the transient pumping Ni-like Mo laser at $\lambda = 18.9$ nm [31] to 5.5 ps for the OFI-pumped Ni-like Kr laser at $\lambda = 32.8$ nm [27]. This shorter coherence time is correspondingly and physically related to a spectral width that is $\sim$3–10 times larger, and is the result of the QSS zinc laser being operated at both higher electron density and higher ionic temperature. Such a feature is also supported by the few earlier measurements of QSS-pumped XUV laser linewidth reported by other authors in the mid-1990s [43–45]. Table I summarizes the spectral widths measured in these earlier works compared to the measurement presented here. Although this comparison is useful, it should be kept in mind that the experiments differ

TABLE I. Comparison of the measured spectral widths of the present work and earlier works for the same laser transition.

Element	λ_0(nm)	Reference	$G\,L$	$\Delta\nu$(Hz)	τ_c(ps)
Zn	21.2	[This work]	$\sim$15 (sat.)	7.8×10^{11}	0.68
Se	18.2	[43]	10	1.2×10^{12}	0.45
Ge	19.6	[44]	5	2.0×10^{12}	0.27
Y	15.5	[45]	$\sim$20 (sat.)	1.6×10^{12}	0.33

by several aspects, which we will briefly summarize, so that a strict quantitative comparison of the $\Delta\nu$ values given in Table I would not be relevant. The first difference relates to the measurement method. In the works by Koch *et al.* [43] and Yuan *et al.* [44] the measurement was made directly in the spectral domain, using a high-resolution grating spectrometer. The measurement reported in [45] was based on the same method of temporal autocorrelation of the XUV laser field used in the present work, but with an amplitude-division interferometer involving XUV multilayer beamsplitters. The second difference relates to the element used to generate the XUV laser plasma. All the results shown in Table I relate to the same transition $(2p^5_{1/2}3p_{1/2})_{J=0} \rightarrow (2p^5_{1/2}3s_{1/2})_{J=1}$ as the one considered in Ne-like Zn in this work, but the experiments were done with different elements at different lasing wavelengths: $\lambda = 18.2$ nm in Ne-like Se [43], $\lambda = 19.6$ nm in Ne-like Ge [44], and $\lambda = 15.5$ nm in Ne-like Y [45]. Note that the latter element is a particular case as the $(2p^5_{1/2}3p_{1/2})_{J=0} \rightarrow (2p^5_{1/2}3s_{1/2})_{J=1}$ line in Ne-like yttrium is blended with another component $(2p^5_{3/2}3p_{3/2})_{J=2} \rightarrow (2p^5_{3/2}3s_{1/2})_{J=1}$ of the same $3p-3s$ transition array [46]. Although in all the experiments the XUV laser plasma was pumped in the QSS regime, the parameters of the pump laser were slightly different. In particular, in [45] the yttrium plasma was generated with a frequency-doubled laser pulse ($\lambda = 0.53\ \mu$m), leading to an increased electron density (Ne $\sim 1.2 \times 10^{21}$cm^{-3} [47]) in the gain zone. Finally different gain-length product ($G\,L$) values were achieved in each experiment; they are indicated in Table I. This information is particularly relevant since, as will be discussed in detail in the next section, the width of the XUV laser line exhibits a strong decreasing dependence with $G\,L$ ($\Delta\nu \propto 1/\sqrt{G\,L}$) due to gain narrowing. This narrowing slows down when the amplification enters the saturation regime [43] reaching a typical value $\Delta\nu_{\rm sat} \approx \Delta\nu_0/\sqrt{(G\,L)_{\rm sat}} \approx \Delta\nu_0/4$. While saturation was achieved in our work, as well as in the work by Celliers *et al.*, the measurements in Se and Ge correspond to smaller $G\,L$, significantly below saturation.

Keeping in mind all these different experimental conditions, several trends can be pointed out from the comparison of the measured linewidths summarized in Table I. First, our measurement in Ne-like zinc is consistent with the results obtained in Ne-like selenium and Ne-like germanium, if we take into account the different values of $G\,L$, as will be shown in the next section. Second, a larger saturated linewidth is observed in the saturated Ne-like yttrium laser, which was generated at a slightly higher electron density with a 2ω pump laser pulse. Finally, all the measured linewidths correspond to coherence times (shown in the last column in Table I) that are significantly shorter than 1 ps. Compared to the other types of collisional XUV lasers, namely based on OFI, transient or capillary-discharge pumping, QSS-pumped XUV lasers thus appear to have a broader spectral linewidth, which is more favorable to the amplification of a seed pulse with a femtosecond time scale.

IV. SPECTRAL GAIN NARROWING

The measurement discussed in the previous section was done for a 3-cm-long Zn plasma and a double-pass configuration for which, as it will be shown later, saturation is reached. In order to obtain a more detailed knowledge about the spectral properties of the Zn plasma amplifier we carried out two additional series of measurements in which the zinc laser was operated in single pass, in the small-signal gain regime (below saturation), for two different plasma lengths: 2 and 3 cm. Below saturation, the amplified intensity drops down exponentially when the plasma length is shortened, so that it was not possible to extend the measurement to plasmas shorter than 2 cm due to a weak level of signal. The main goal of these measurements was to investigate the gain narrowing of the spectral line, from which more detailed information about the broadening of the line before amplification can be extracted and compared to the predictions of numerical simulations. For both series, the measured autocorrelation signal was fitted with a Gaussian function, from which coherence times of $\tau_c = 480 \pm 30$ fs and $\tau_c = 440 \pm 110$ fs were inferred for the 3-cm- and 2-cm-long targets, respectively. The corresponding spectral bandwidths are $\Delta\nu = 1.1 \pm 0.1 \times 10^{12}$ Hz for the 2-cm plasma and $\Delta\nu = 1.2 \pm 0.3 \times 10^{12}$ Hz for the 3-cm plasma. Both these $\Delta\nu$ values are close, but significantly larger than the one found in the double-pass configuration, showing clear evidence of gain narrowing for the longest amplification length. These results were compared to the predictions of a one-dimensional (1D) model simulation that calculates the frequency-dependent intensity of the XUV laser line along the plasma amplifier, taking into account Doppler and collisional broadening, and gain saturation. More precisely, the model solves the following time-independent, unidirectional radiative transfer equation [43]:

$$\frac{d\mathcal{I}}{dz}(\nu,z) = \frac{J_0}{V(\nu_0)}\left[1 + \frac{g_0}{J_0}\mathcal{I}(\nu,z)\right] \times \int_0^\infty \frac{S(u)\phi(\nu,u)du}{1+\int_0^\infty \mathcal{I}(\nu')\phi(\nu',u)d\nu'}, \qquad (1)$$

where $\mathcal{I}(\nu,z)$ and J_0 are normalized to the saturation intensity $I_{\rm sat}$: $\mathcal{I}(\nu,z) = I(\nu,z)/I_{\rm sat}$, $J_0 = j_0/I_{\rm sat}$. $I(\nu,z)$ is the spectral intensity along the positive direction of amplification z, j_0, and g_0 are, respectively, the emissivity and gain at line center. $S(u)$ and $\phi(u)$ are, respectively, the normalized inhomogeneous (Gaussian) and homogeneous (Lorentzian) intrinsic line profiles, and $V(\nu_0)$ is the normalized Voigt profile resulting from their convolution. The width of the Gaussian and Lorentzian components were computed from the PPP lineshape code, a multielectron radiator line broadening code developed to calculate spectral line profiles for a general emitter in a plasma [48], for a range of electron temperature and density, and ion temperature relevant to the Zn XUV amplifier. The normalized emissivity $J_0 = j_0/I_{\rm sat}$ was computed for the same plasma conditions using atomic data from the literature: $J_0 = 5.5 \times 10^{-7}$.

The gain coefficient g_0 was experimentally determined by measuring the time-integrated signal from the single-pass zinc laser for plasma lengths of 2, 2.5, and 3 cm from beam footprint images recorded at 2.5 m from the source (see Fig. 1). The measured experimental data, shown in Fig. 3, were fitted with the usual Linford formula [49], which describes the spectrally integrated output intensity of the XUV laser as a function of length in the small-signal gain regime. The fit yields a gain

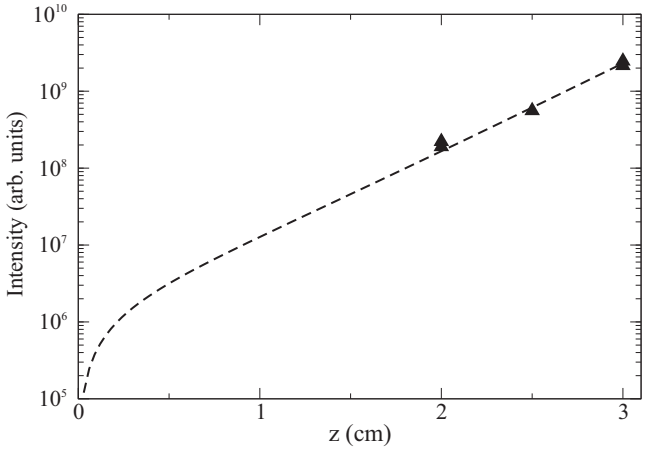

FIG. 3. Output intensity of the single-pass Ne-like Zn laser versus plasma length. The experimental data are fitted with the Linford function, yielding a gain $g_0 = 2.83 \pm 0.36$ cm^{-1}.

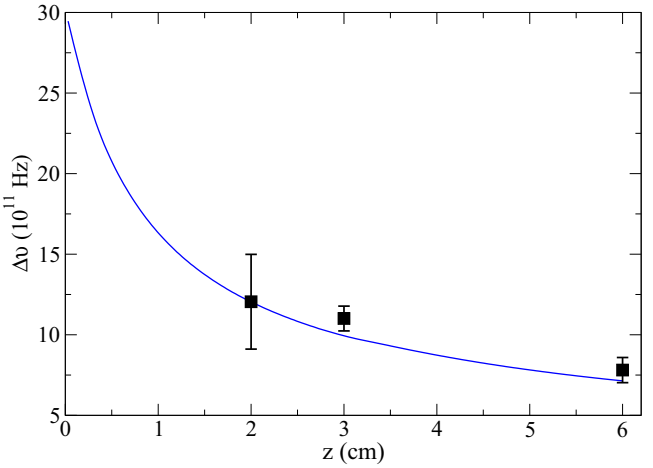

FIG. 4. (Color online) (Black squares) Measured linewidth $\Delta\nu$ for three different amplification lengths: 2 and 3 cm in single pass and 6 cm in double pass. The experimental data are well reproduced by the 1D-radiative transfer calculation (solid line) using the experimentally measured gain as an input value.

$g_0 = 2.83 \pm 0.36$ cm^{-1}. This value is significantly smaller than the gain of ~7 cm^{-1} evaluated earlier for the same XUV laser [36], likely due to less optimal pumping conditions.

Equation (1), which accounts for saturation effects, can also be used to calculate the output intensity and the spectral width of the lasing line in the double-pass configuration. In this case, the frequency-dependent intensity calculated at the output of a first 3-cm plasma is multiplied by an effective (frequency-independent) coupling efficiency factor R_{eff} before being injected in the second 3-cm plasma. The coupling efficiency factor R_{eff} includes the reflectivity of the half-cavity mirror ($R = 30\%$) as well as geometrical losses [36]. Taking a beam divergence of 5 mrad and a gain region size of 100 μm × 50 μm would lead to ~20% of the reflected beam being effectively re-injected in the gain region and $R_{\text{eff}} \sim 6\%$. The value of R_{eff} can also be estimated by adjusting it until the calculated ratio between double-pass and single-pass intensities, computed from the radiative transfer simulation, equals to the experimental one. An experimental ratio of ~6.6 was measured from the interferogram images obtained in double-pass and in single-pass configurations, by integrating the signal over the area intercepted by the mirrors. The value of R_{eff} inferred with this method is smaller ($R_{\text{eff}} \sim 0.3$ %). It should be noted, however, that the calculations of the evolution of $\Delta\nu$ presented below are not significantly affected by the value of R_{eff}. Our radiation transfer calculations also indicate that the output intensity in double-pass configuration is saturated, even for this small value of R_{eff}. Close to the output of the plasma during the second pass, the computed gain is reduced to $g_{2-\text{pass}} \approx 0.86\text{cm}^{-1}$, i.e., ~30% of the small-signal gain value.

The linewidths inferred from the measurements in single-pass and double-pass configurations are plotted in Fig. 4. The data are well reproduced by the results of our model simulation (solid line) based on Eq. (1), in which the measured values $g_0 = 2.83\text{cm}^{-1}$ and $R_{\text{eff}} = 0.3\%$ were used as input data. As mentioned earlier, the value of R_{eff} has a negligible effect on the bandwidth calculated in double-pass (i.e., for $3\text{cm} < z \leqslant 6\text{cm}$). Taking $R_{\text{eff}} = 6\%$ as considered above would result in a calculated $\Delta\nu$ at $z = 6$ cm that is only ~0.4 % narrower than the one plotted in Fig. 4, and would thus still fall within the experimental error bar. The best agreement with the experimental data was found by adjusting the intrinsic linewidth $\Delta\nu$ (at $z = 0$) to 2.9×10^{12} Hz, with an homogeneous (Lorentzian) component of 1.7×10^{12} Hz and an inhomogeneous (Gaussian) component of 1.9×10^{12} Hz, corresponding to $N_e = 5.5 \times 10^{20}$ cm^{-3}, $kT_e = 300$ eV, $kT_i = 200$ eV.

As noted in the previous section, our measured linewidths are consistent with those measured in Ne-like Se by Koch *et al.* [43], which were also measured for different plasma lengths. This can be seen in Fig. 5, where both sets of data are plotted versus a common gain-length product horizontal

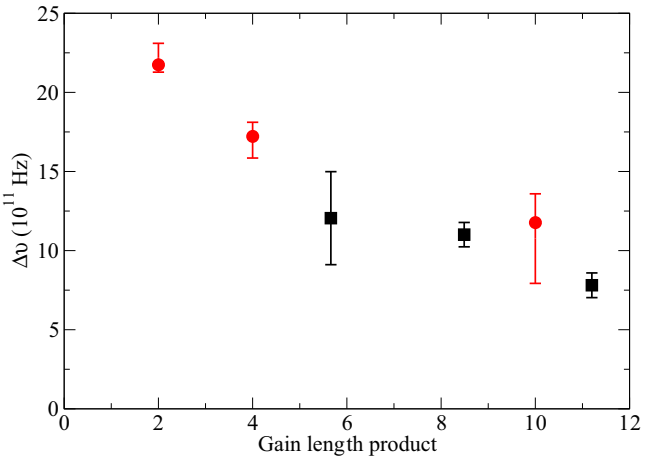

FIG. 5. (Color online) (Black squares) Same data as in Fig. 4, but plotted as a function of the gain-length product. For the largest $G\,L$ corresponding to the double-pass configuration, an effective value is used. (Red full circles) Adapted from [43] (Fig. 11), measured linewidths in Ne-like Se. Although the two sets of data were obtained from distinct methods, they exhibit a very good consistency.

scale. For the double-pass case we have used an effective gain-length value estimated from the relation [36] $(G\,L)_{\rm eff} = 2g_0L + \ln(R_{\rm eff}) \approx 11$. The Se data were adapted from Fig. 11 in [43]. The intrinsic linewidth evaluated by the authors from their measurements is $\Delta\nu_0 = 2.9 \times 10^{12}$ Hz, similar to the one we used to simulate our experimental data. It should be reminded that the measurements in Se were made directly in the frequency domain, using a high-resolution spectrometer.

Using the 1D-radiative transfer code with the same gain and spectral bandwidth as measured for the Zn laser line we have simulated the amplification of an external seed having a ∼50 times broader spectral width ($\Delta\lambda/\lambda = 10^{-2}$). At the output of the 6-cm plasma (double pass), the spectral width of the amplified seed is calculated to be ∼4.5% larger than the ASE one, thus consistent with a pulse duration of ∼500 fs.

V. CONCLUSIONS

In conclusion, we have carried out a detailed characterization of the temporal coherence and spectral bandwidth of the Ne-like Zn XUV laser generated at PALS in the QSS pumping regime and operated either below or above saturation. In all cases, the measured coherence times are significantly below 1 ps. The QSS zinc XUV laser is found to have a broader bandwidth than the previously investigated collisional XUV lasers, due to its more favorable plasma conditions for spectral broadening. Gain narrowing of the lasing line was also observed. The measured data are consistent with radiative transfer calculations using the gain values measured during the same experimental campaign. Finally, the spectral bandwidth of the zinc XUV laser appears to be compatible with an efficient adiabatic amplification of subpicosecond pulses which could be generated by seeding it with a femtosecond high-order harmonic pulse.

ACKNOWLEDGMENTS

This work has received funding from EC's Seventh Framework Programme (LASERLAB-EUROPE, Grant Agreement No. 284464, and ELI: EXTREME LIGHT INFRASTRUCTURE Project No. CZ.1.05/1.1.00/02.0061), as well as from ECOP (Projects No. CZ.1.07/2.3.00/30.0057 and No. CZ.1.07/2.3.00/20.0279).

[1] J. Feldhaus, J. Arthur, and J. B. Hastings, J. Phys. B: At. Mol. Opt. **38**, S799 (2005).
[2] E. Allaria, R. Appio, L. Badano, W. Barletta, S. Bassanese, S. Biedron, A. Borga, E. Busetto, D. Castronovo, P. Cinquegrana *et al.*, Nat. Photonics **6**, 699 (2012).
[3] K. Midorikawa, Y. Nabekawa, and A. Suda, Prog. Quantum Electron. **32**, 43 (2008).
[4] S. Suckewer and P. Jaegle, Laser Phys. Lett. **6**, 411 (2009).
[5] B. Nagler, U. Zastrau, R. R. Fäustlin, S. M. Vinko, T. Whitcher, A. Nelson, R. Sobierajski, J. Krzywinski, J. Chalupsky, E. Abreu *et al.*, Nat. Phys. **5**, 693 (2009).
[6] C. Bostedt, E. Eremina, D. Rupp, M. Adolph, H. Thomas, M. Hoener, A. De Castro, J. Tiggesbäumker, K.-H. Meiwes-Broer, T. Laarmann *et al.*, Phys. Rev. Lett. **108**, 093401 (2012).
[7] S. Baker, J. S. Robinson, C. Haworth, H. Teng, R. Smith, C. Chirilă, M. Lein, J. Tisch, and J. Marangos, Science **312**, 424 (2006).
[8] R. Kienberger, E. Goulielmakis, M. Uiberacker, A. Baltuska, V. Yakovlev, F. Bammer, A. Scrinzi, T. Westerwalbesloh, U. Kleineberg, U. Heinzmann *et al.*, Nature (London) **427**, 817 (2004).
[9] C. La-O-Vorakiat, M. Siemens, M. M. Murnane, H. C. Kapteyn, S. Mathias, M. Aeschlimann, P. Grychtol, R. Adam, C. M. Schneider, J. M. Shaw, H. Nembach, and T. J. Silva, Phys. Rev. Lett. **103**, 257402 (2009).
[10] H. Tang, O. Guilbaud, G. Jamelot, D. Ros, A. Klisnick, D. Joyeux, D. Phalippou, M. Kado, M. Nishikino, M. Kishimoto *et al.*, Appl. Phys. B **78**, 975 (2004).
[11] J. Nejdl, M. Kozlová, T. Mocek, and B. Rus, Phys. Plasmas **17**, 122705 (2010).
[12] L. Gartside, G. Tallents, A. Rossall, E. Wagenaars, D. Whittaker, M. Kozlová, J. Nejdl, M. Sawicka, J. Polan, M. Kalal *et al.*, High Energy Density Phys. **7**, 91 (2011).
[13] L. Urbanski, A. Isoyan, A. Stein, J. Rocca, C. Menoni, and M. Marconi, Opt. Lett. **37**, 3633 (2012).
[14] S. Heinbuch, F. Dong, J. Rocca, and E. Bernstein, J. Chem. Phys. **126**, 244301 (2007).
[15] B. A. Reagan, M. Berrill, K. A. Wernsing, C. Baumgarten, M. Woolston, and J. J. Rocca, Phys. Rev. A **89**, 053820 (2014).
[16] R. A. Banici, G. V. Cojocaru, R. G. Ungureanu, R. Dabu, D. Ursescu, and H. Stiel, Opt. Lett. **37**, 5130 (2012).
[17] O. Delmas, M. Pittman, K. Cassou, O. Guilbaud, S. Kazamias, G. V. Cojocaru, O. Neveu, J. Demailly, E. Baynard, D. Ursescu *et al.*, Opt. Lett. **39**, 6102 (2014).
[18] F. Staub, C. Imesch, D. Bleiner, and J. Balmer, Opt. Commun. **285**, 2118 (2012).
[19] M. Berrill, D. Alessi, Y. Wang, S. R. Domingue, D. H. Martz, B. M. Luther, Y. Liu, and J. J. Rocca, Opt. Lett. **35**, 2317 (2010).
[20] J. P. Goddet, S. Sebban, J. Gautier, P. Zeitoun, C. Valentin, F. Tissandier, T. Marchenko, G. Lambert, M. Ribières, D. Douillet *et al.*, Opt. Lett. **34**, 2438 (2009).
[21] S. Ackermann, A. Azima, S. Bajt, J. Bödewadt, F. Curbis, H. Dachraoui, H. Delsim-Hashemi, M. Drescher, S. Düsterer, B. Faatz *et al.*, Phys. Rev. Lett. **111**, 114801 (2013).
[22] T. Ditmire, M. Hutchinson, M. Key, C. Lewis, A. MacPhee, I. Mercer, D. Neely, M. Perry, R. Smith, J. Wark *et al.*, Phys. Rev. A **51**, R4337(R) (1995).
[23] P. Zeitoun, G. Faivre, S. Sebban, T. Mocek, A. Hallou, M. Fajardo, D. Aubert, P. Balcou, F. Burgy, D. Douillet *et al.*, Nature (London) **431**, 426 (2004).
[24] Y. Wang, E. Granados, M. A. Larotonda, M. Berrill, B. M. Luther, D. Patel, C. S. Menoni, and J. J. Rocca, Phys. Rev. Lett. **97**, 123901 (2006).
[25] O. Guilbaud, S. Kazamias, K. Cassou, O. Delmas, J. Demailly, O. Neveu, D. Ros, E. Baynard, M. Pittman, M. Shazad, A. Rossal, G. J. Tallents, A. Le Marec, L. Klisnick, A Lu, P. Zeitoun, G. V. Cojocaru, R. G. Ungureanu, B. R. A, and D. Ursescu, in

14th International Conference on X-Ray Lasers 2014 (Springer Proceedings in Physics, in press, 2015).

[26] Y. Wang, M. Berrill, F. Pedaci, M. M. Shakya, S. Gilbertson, Z. Chang, E. Granados, B. M. Luther, M. A. Larotonda, and J. J. Rocca, Phys. Rev. A **79**, 023810 (2009).

[27] O. Guilbaud, F. Tissandier, J.-P. Goddet, M. Ribière, S. Sebban, J. Gautier, D. Joyeux, D. Ros, K. Cassou, S. Kazamias, A. Klisnick, J. Habib, P. Zeitoun, D. Benredjem, T. Mocek, J. Nedjl, S. de Rossi, G. Maynard, B. Cros, A. Boudaa, and A. Calisti, Opt. Lett. **35**, 1326 (2010).

[28] F. Tissandier, S. Sebban, M. Ribière, J. Gautier, P. Zeitoun, G. Lambert, A. B. Sardinha, J.-P. Goddet, F. Burgy, T. Lefrou *et al.*, Phys. Rev. A **81**, 063833 (2010).

[29] O. Larroche and A. Klisnick, Phys. Rev. A **88**, 033815 (2013).

[30] A. Klisnick, O. Guilbaud, D. Ros, K. Cassou, S. Kazamias, G. Jamelot, J.-C. Lagron, D. Joyeux, D. Phalippou, Y. Lechantre *et al.*, J. Quant. Spectrosc. Radiat. Transfer **99**, 370 (2006).

[31] L. M. Meng, D. Alessi, O. Guilbaud, Y. Wang, M. Berrill, B. Luther, S. R. Domingue, D. H. Martz, D. Joyeux, S. D. Rossi, J. J. Rocca, and A. Klisnick, Opt. Express **19**, 12087 (2011).

[32] L. Urbanski, M. C. Marconi, L. M. Meng, M. Berrill, O. Guilbaud, A. Klisnick, and J. J. Rocca, Phys. Rev. A **85**, 033837 (2012).

[33] A. Calisti, S. Ferri, C. Mossé, B. Talin, A. Klisnick, L. Meng, D. Benredjem, and O. Guilbaud, High Energy Density Phys. **9**, 516 (2013).

[34] A. Depresseux, E. Oliva, J. Gautier, F. Tissandier, J. Nejdl, M. Kozlova, G. Maynard, J. P. Goddet, A. Tafzi, Lifschitz, A. H. T. Kim, S. Jacquemot, V. Malka, K. Ta Phuoc, C. Thaury, P. Rousseau, G. Iaquaniello, T. Lefrou, A. Flacco, B. Vodungbo, G. Lambert, A. Rousse, P. Zeitoun, and S. Sebban, Nat. Photon. (to be published).

[35] E. Oliva, M. Fajardo, L. Li, M. Pittman, T. Le, J. Gautier, G. Lambert, P. Velarde, D. Ros, S. Sebban *et al.*, Nat. Phot. **6**, 764 (2012).

[36] B. Rus, T. Mocek, A. R. Präg, M. Kozlová, G. Jamelot, A. Carillon, D. Ros, D. Joyeux, and D. Phalippou, Phys. Rev. A **66**, 063806 (2002).

[37] L. Meng, A. Klisnick, M. Kozlova, K. Bohacek, M. Krus, J. Prokupek, L. Urbanski, M. Marconi, M. Berrill, J. Rocca *et al.*, in *X-Ray Lasers 2012* (Springer, New York, 2014), pp. 175–180.

[38] B. Rus, Ph.D thesis, Université Paris-Sud, 1995.

[39] F. Polack, D. Joyeux, J. Svatoš, and D. Phalippou, Rev. Sci. Instrum. **66**, 2180 (1995).

[40] R. Mitzner, B. Siemer, M. Neeb, T. Noll, F. Siewert, S. Roling, M. Rutkowski, A. Sorokin, M. Richter, P. Juranic *et al.*, Opt. Express **16**, 19909 (2008).

[41] W. Schlotter, F. Sorgenfrei, T. Beeck, M. Beye, S. Gieschen, H. Meyer, M. Nagasono, A. Föhlisch, and W. Wurth, Opt. Lett. **35**, 372 (2010).

[42] M. Kozlova, J. Nejdl, A. Klisnick, A. Le Marec, L. Meng, F. Tissandier, T. Fok, L. Wegrzynski, A. Bartnik, P. Wachulak *et al.*, in *SPIE Optical Engineering + Applications* (International Society for Optics and Photonics, Bellingham, 2013), pp. 884904–884904.

[43] J. A. Koch, B. J. MacGowan, L. B. Da Silva, D. L. Matthews, J. H. Underwood, P. J. Batson, R. W. Lee, R. A. London, and S. Mrowka, Phys. Rev. A **50**, 1877 (1994).

[44] G. Yuan, Y. Kato, K. Murai, H. Daido, and R. Kodama, J. Appl. Phys. **78**, 3610 (1995).

[45] P. Celliers, F. Weber, L. Da Silva, T. Barbee, R. Cauble, A. Wan, and J. Moreno, Opt. Lett. **20**, 1907 (1995).

[46] P. Holden, M. Nantel, B. Rus, and A. Sureau, J. Phys. B: At. Mol. Opt. **28**, 1369 (1995).

[47] L. Da Silva, B. J. MacGowan, S. Mrowka, J. Koch, R. A. London, D. L. Matthews, and J. H. Underwood, Opt. Lett. **18**, 1174 (1993).

[48] A. Calisti, F. Khelfaoui, R. Stamm, B. Talin, and R. W. Lee, Phys. Rev. A **42**, 5433 (1990).

[49] G. J. Linford, E. R. Peressini, W. R. Sooy, and M. L. Spaeth, Appl. Opt. **13**, 379 (1974).